Optimal design of robust piezoelectric unimorph microgrippers

Ruiz, David; Díaz-Molina, Alex ; Sigmund, Ole; Donoso, Alberto; Carlos Bellido, José ; Sánchez-Rojas, José Luis

Published in:
Applied Mathematical Modelling

Link to article, DOI:
10.1016/j.apm.2017.10.024

Publication date:
2018

Document Version
Peer reviewed version

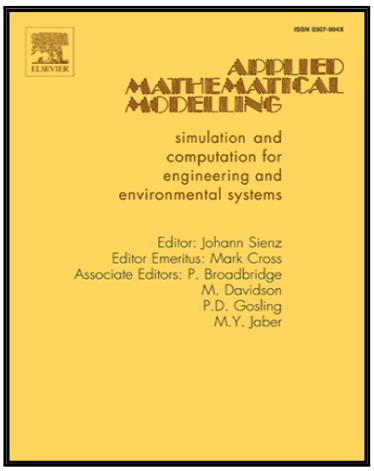

Optimal design of robust piezoelectric unimorph microgrippers

David Ruiz, Alex Díaz-Molina, Ole Sigmund, Alberto Donoso,
José Carlos Bellido, José Luis Sánchez-Rojas

PII: S0307-904X(17)30641-8
DOI: 10.1016/j.apm.2017.10.024
Reference: APM 12025

To appear in: *Applied Mathematical Modelling*

Received date: 25 March 2017
Revised date: 5 October 2017
Accepted date: 18 October 2017

Please cite this article as: David Ruiz, Alex Díaz-Molina, Ole Sigmund, Alberto Donoso, José Carlos Bellido, José Luis Sánchez-Rojas, Optimal design of robust piezoelectric unimorph microgrippers, *Applied Mathematical Modelling* (2017), doi: 10.1016/j.apm.2017.10.024

Highlights

- Systematic procedure to design piezoelectric actuated microgrippers.
- Simultaneous optimization of the host structure and the polarization profile.
- Out-of-plane bending produced is suppressed in some points of interest.
- Control of the feature size throught robust approach.
- Minimization of target to small manufacturing errors.

Optimal design of robust piezoelectric unimorph microgrippers

David Ruiz[a], Alex Díaz-Molina[b], Ole Sigmund[c], Alberto Donoso[a], José Carlos Bellido[a], José Luis Sánchez-Rojas[b]

[a] *Departamento de Matemáticas, ETSII Universidad de Castilla-La Mancha, 13071 Ciudad Real, Spain*
[b] *Microsystems Actuators and Sensors Group, ETSII Universidad de Castilla-La Mancha, 13071 Ciudad Real, Spain*
[c] *Department of Mechanical Engineering, Technical University of Denmark, 2800 Kgs. Lyngby, Denmark*

Abstract

Topology optimization can be used to design piezoelectric actuators by simultaneous design of host structure and polarization profile. Subsequent micro-scale fabrication leads us to overcome important manufacturing limitations: difficulties in placing a piezoelectric layer on both top and bottom of the host layer. Unsymmetrical layer placement makes the actuator bend, spoiling the predicted performance of the device. The aim of this work is to maximize the in-plane displacement of a microgripper-type actuator while out-of-plane displacement at some points of interest is suppressed. This last issue is the main novelty introduced in this work, and the emphasis is placed on the modelling and its applicability rather than numerical methods. In addition, a robust formulation of the problem has been used in order to ensure minimum length scale in the optimal designs, which it is crucial from the manufacturability point of view.

Keywords: Piezoelectric unimorph actuators, Topology optimization, Robust formulation

*Corresponding author
Email address: David.Ruiz@uclm.es (David Ruiz)

1. Introduction

Nowadays topology optimization is considered a major conceptual tool not only for structural design, but also, among others, for compliant mechanisms design or even metamaterials.

In the last years, many authors have also applied the topology optimization method to piezoelectric devices, leading to improved physical responses in different contexts. A pioneering work where topology optimization is used to optimize piezoelectric structures is [1], where the authors designed 1-3 composites for hydrophone applications. More specifically, regarding the design of in-plane piezoelectric actuators using topology optimization, a work was due to [2], where the host structure is optimized while the piezoelectric layer is kept fixed. Since then, the list of works related to this topic has grown immensely, and we just mention some of them. [3] considered the optimization of the piezoelectric part together with the polarization based on a three layer model. [4] and [5] optimized at the same time the host structure and the piezoelectric distribution. In [6] the host structure and the piezoelectric layers were optimized simultaneously, but also included a spatial distribution of the control voltage (related to the polarization of the piezoelectric layers). These authors improved their results in [7] by introducing an interpolation scheme in the tri-level actuation voltage term. New results are presented in [8] and [9] for in-plane and out-of-plane piezoelectric transducers, respectively. Another recent reference on simultaneous optimization of structure and piezoelectric profile in the actuators context is [10].

Also recently, a systematic method for optimizing effective transducers for statics and mode filtering is presented in [11] and [12], respectively. In both works, the goal is achieved by simultaneously optimizing both the host structure (that includes piezoelectric layers) and the polarization profile of the electrodes. The model considers two piezoelectric layers perfectly bonded to both sides of the host plate-type structure. Either in-phase or out-of-phase polarization of the two piezo layers makes the structure move in-plane or out-of-plane, respec-

tively. Unfortunately, at the micro-scale and due to the current constraints in both surface and bulk micromachining techniques, a piezoelectric layer below the structural silicon layer requires complex processing techniques ([13]), and hence only one piezoelectric film can be deposited on top of the structure. When fabricating a sensor this fact is not truly a problem, since the deformation is produced by an external force. However, the main problem appears for actuators. With only one piezoelectric layer, it moves both in the in-plane and out-of-plane directions.

Motivated by this real difficulty, this work is intended as a continuation of [11], but taking into account that just one piezoelectric layer will be placed on the host structure. This new model includes new constraints avoiding structure bending at certain points of interest. In addition, and having manufacturability in mind, the so-called robust formulation ([14]) is implemented in the model with two purposes: the first one, controlling the minimum length scale in both solid and void regions; and the second one, minimizing the sensitivity of the target of the microactuator under fabrication errors. Since the expected displacements are small compared to the size of the actuator, a linear elasticity model is used. In [15] nonlinear modelling is utilized in order to model piezo MEMS exhibiting large displacements. We would like to remark the novelty of the modelling motivated by manufacturing limitations and use of piezoelectric microgrippers, so that the emphasis is placed on the mathematical model and its applicability rather than numerical methods implemented to simulate the problem.

The paper is organized as follows. In Section 2 the continuous formulation of the model is presented, followed by the discrete formulation. Section 3 is dedicated to briefly introduce the concept of robust topology optimization. In Section 4, the algorithm used to solve the problem is described. The solutions obtained with Matlab and corroborated with CoventorWare[1] are shown in Section 5. Finally, Section 6 is devoted to conclusions and future works.

[1] www.coventor.com

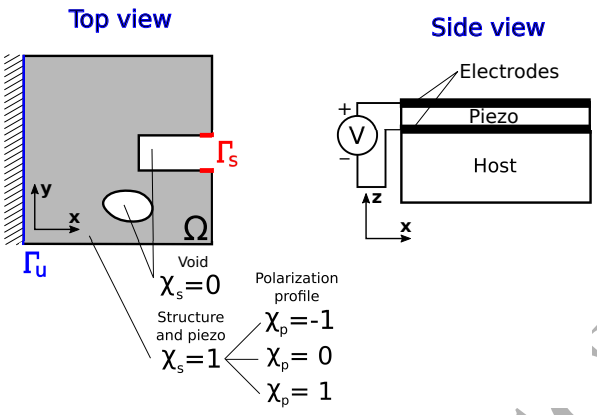

Figure 1: Top and side view of the layered structure.

2. Formulation of the problem

2.1. Continuous formulation

As a design domain Ω we consider a rectangular plate clamped at its left side. The host structure is perfectly bonded with a top piezoelectric layer (that is sandwiched between two electrodes) of negligible stiffness compared to the plate. This configuration is shown in Fig.1. Γ_u stands for the left clamped side of the boundary of Ω.

Whenever applying a voltage, the electrodes polarize the piezoelectric layer, and the electric field generates, through the piezoelectric effect, a mechanical stress over this layer, which in turn deforms the host structure. The objective of the problem is the maximization of the y-displacement on the part of the boundary of Ω called Γ_s. The unsymmetrical configuration of the layers of the plate make the device bend in the out-of-plane direction, disturbing the in-plane behaviour. In order to overcome this issue, the out-of-plane deformation in the z-axis on Γ_s must be suppressed. Two design variables are used in our problem. χ_s is a characteristic function, $\chi_s \in \{0, 1\}$, that represents the structure layout ($\chi_s = 1$) and void ($\chi_s = 0$), as usual. χ_p is also a discrete function such that $\chi_p \in \{-1, 0, 1\}$, meaning negative, null or positive polarity.

It is important to remark that the role of the latter variable is crucial here

because deformations at a certain point are precisely controlled by the polarity of the electrode. Those parts of the structure that are not being covered by electrode are not electrically affected. Actually, it was shown in [16] that optimal solutions will be covered of electrode all along the structure, so that χ_p will never be zero in the optimum for the planar case.

The continuous problem formulation may be written as:

$$\max_{\chi_s,\chi_p} : \quad v_{|\Gamma_s}$$

s.t.:

In-plane equilibrium equation:

$$\begin{cases} -\mathrm{div}\big(E_s\chi_s\varepsilon(u,v)\big) = -\mathrm{div}\big(E_s\chi_s\varepsilon_0(\chi_s,\chi_p)\big) & \\ & \text{in } \Omega \\ \big(E_s\chi_s\varepsilon(u,v)\big)\cdot\mathbf{n} + \mathbf{K}\cdot(u,v) = 0, & \text{on } \Gamma_s \\ u,\, v = 0, & \text{on } \Gamma_u \end{cases}$$

Out-of-plane equilibrium equation:

$$\begin{cases} \nabla^2\left(\frac{E_s\chi_s t^3}{12(1-\nu^2)}\nabla^2 w\right) = \chi_s\left[M_0\Delta(\chi_p)\right] & \text{in } \Omega \\ w = 0, & \text{on } \Gamma_u \end{cases}$$

Constraints:

$$\begin{aligned} &\tfrac{1}{|\Omega|}\textstyle\int_\Omega \chi_s \,\mathrm{d}x\,\mathrm{d}y \le V_0 \\ &w^2_{|\Gamma_s} \le \varepsilon_d^2 v^2_{|\Gamma_s} \\ &\chi_s \in \{0,1\} \\ &\chi_p \in \{-1,0,1\}, \end{aligned}$$

where $v_{|\Gamma_s}$ is the restriction of the second component of the solution of the in-plane model to Γ_s. E_s and ν the stiffness (fourth-order tensor) and Poisson's ratio of the host structure material, respectively, t is the plate thickness, and ε is the symmetric strain tensor. ε_0 and M_0 are the initial strain and the moment

produced by the piezoelectric force, respectively (this will be commented below in Section 2.2). $\mathbf{K} = (0, k_{out})$ is the spring stiffness vector (bold case letter is used for vectors) that models the output, $\mathbf{n}$ is the normal outer vector to the boundary of Ω, V_0 is the maximum volume fraction of allowed material and ε_d is a small value that relates the displacements to be optimized and suppressed. Note that a very small value of this coefficient leads to lack of solution, obtaining designs that do not satisfy the constraints on the vertical deformation of the gripper.

The constraints over the vertical displacement are formulated in terms of the in-plane displacement. This is made in order to avoid the dependence of the displacements on the size of the gripper, but these restrictions can be fixed for a particular case with a constant value.

We would like to mention that the mathematical formulation of the out-of-plane equilibrium equation for a piezoelectric actuator like the one considered here, i.e. the piezoelectric actuator distributed in patches along the plate, can be found for instance in [17] and [18]. The formulation given here for the source term looks different than in those references, but indeed the term

$$\Delta(\chi_p),$$

is equal (in the sense of distribution) to that appearing in those references, namely the normal derivative

$$\chi_p \frac{\partial \delta_\gamma}{\partial \boldsymbol{\nu}},$$

where γ is the curve separating the patches, i.e. the subsets of Ω where χ_p takes different values on (recall that $\chi_p \in \{-1, 0, 1\}$), δ_γ is the Dirac mass supported on γ (i.e., the measure supported on γ with total measure 1), and $\boldsymbol{\nu}$ is the outer normal vector to the patches.

2.2. Discrete formulation

As usual, topology optimization problems lack of classical solutions, so first the discrete optimizations variables, χ_s, χ_p have necessarily to be relaxed into continuous densities $\rho_s \in [0, 1]$ and $\rho_p \in [-1, 1]$, and afterwards discretized into

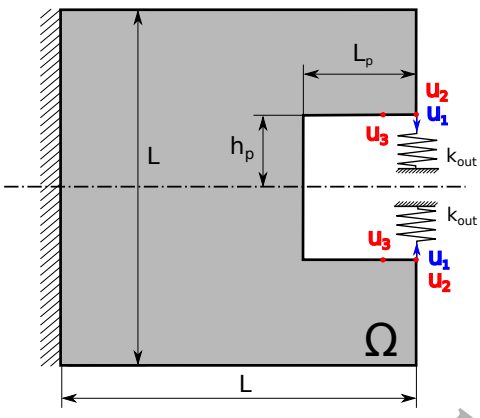

Figure 2: Design domain of the microgripper.

n_e finite elements with two variables per element. Thus, the discrete problem, in the usual topology optimization format, may be written as

$$\max_{\boldsymbol{\rho}_s, \boldsymbol{\rho}_p} : \quad u_1\big(\bar{\boldsymbol{\rho}}_s(\boldsymbol{\rho}_s), \boldsymbol{\rho}_p\big)$$

s.t.: *In-plane and out-of-plane equilibrium equations:*

$$\begin{cases} \big(\mathbf{K}_i(\bar{\boldsymbol{\rho}}_s) + \mathbf{1}_{out} k_{out}\big)\mathbf{U}_i = \mathbf{F}_i(\bar{\boldsymbol{\rho}}_s, \boldsymbol{\rho}_p) \\ \mathbf{K}_o(\bar{\boldsymbol{\rho}}_s)\mathbf{U}_o = \mathbf{F}_o(\bar{\boldsymbol{\rho}}_s, \boldsymbol{\rho}_p) \end{cases}$$

Displacements at the jaws:

$$\begin{cases} u_1 = \mathbf{L}_1^T \mathbf{U}_i \\ u_2 = \mathbf{L}_2^T \mathbf{U}_o \\ u_3 = \mathbf{L}_3^T \mathbf{U}_o \end{cases}$$

Constraints:

$$
\begin{aligned}
&u_2^2 \leq \varepsilon_d^2 u_1^2 \\
&u_3^2 \leq \varepsilon_d^2 u_1^2 \\
&\mathbf{v}^T \boldsymbol{\rho}_s \leq V_0 \\
&\boldsymbol{\rho}_s \in [0, 1] \\
&\boldsymbol{\rho}_p \in [-1, 1],
\end{aligned}
$$

where u_1 is the in-plane displacement to be maximized, and u_2 and u_3 are the out-of-plane displacements to be suppressed (see Figure 2). $\mathbf{L}_1$ $\mathbf{L}_2$ and $\mathbf{L}_3$ are vectors of zeros with 1 in the element corresponding to the degree of freedom of interest. Subscript i is used for the in-plane case, and o for the out-of-plane one, therefore $\mathbf{K}_i$, $\mathbf{K}_o$ are the global stiffness matrices for the in-plane and out-of-plane cases, respectively. $\mathbf{1}_{out}$ is a zero matrix with a 1 in the degree of freedom to be maximized, k_{out} is the stiffness that models the output, $\mathbf{U}_i$ and $\mathbf{U}_o$ are the global displacement vectors, $\mathbf{F}_i$ and $\mathbf{F}_o$ are the global piezoelectric force vectors, $\mathbf{v}$ is the vector containing the finite element volumes, and V_0 is the maximum volume fraction allowed. At this point it is important to remark that in the discrete approach u_1 is referred to the y-axis displacement and u_2 and u_3 represents vertical displacements over the z-axis, associated with the out-of-plane case.

A scheme of the optimization domain including boundary conditions and loads is given in Fig.2.

As mentioned above, the optimization variables are $\boldsymbol{\rho}_s$ and $\boldsymbol{\rho}_p$, the structure layout and the polarization profile, respectively. Finally, $\bar{\boldsymbol{\rho}}_s$ is the physical density, which is a new (regularized) density obtained from $\boldsymbol{\rho}_s$ after a combined filtering and projection processes. The procedure for obtaining this physical density is explained next.

The SIMP approach does not circumvent the mesh-dependence issue by itself, the design may contain features comparable with the mesh size. In order to alleviate this issue filtering techniques are required. The one used in this work

is a density-based filter (introduced in [19] and [20]). If the structural density is represented by using this filtering approach, gray areas, which are difficult to interpret, can appear in the optimized designs. In order to force 0/1 solutions, a projection approach is used. The projection used is a generalization of previous projections schemes suggested in [21] and [22], and is expressed as follows

$$\bar{\rho}_s^{(e)} = \frac{\tanh(\beta\eta) + \tanh\big(\beta(\tilde{\rho}_s^{(e)} - \eta)\big)}{\tanh(\beta\eta) + \tanh\big(\beta(1-\eta)\big)}, \quad \forall e$$

where β is a tunable parameter that defines the smoothness of the projection and η is the threshold, which can take values between 0 and 1. All the filtered densities $\tilde{\rho}_i$ whose value is lower than η are projected to 0, and the ones whose value is bigger than this parameter are projected to 1. In [23], it is numerically proved that formulating the design problem by using the robust approach (using more than one projection) we can avoid hinges, then ensuring length scale control.

The filtered density $\rho_s^{(e)}$ for each element is computed as follows

$$\tilde{\rho}_s^{(e)} = \frac{\sum_{i \in n_e} \omega(\mathbf{x}_i) v_i \rho_s^{(i)}}{\sum_{i \in n_e} \omega(\mathbf{x}_i) v_i}$$

where v_i is the volume of the i-th element and the weight function $\omega(\mathbf{x}_i)$ is the linearly decaying function

$$\omega(\mathbf{x}_i) = r - ||\mathbf{x}_i - \mathbf{x}_e||$$

with $\mathbf{x}_i$ and $\mathbf{x}_e$ containing the central coordinates of the design cells.

As usual, the modified SIMP method ([24]) is required in order to avoid intermediate values in the structural density. The Youngs modulus of each element is made to be dependent on the element density using this approach. The element stiffness matrix can be formulated as:

$$\mathbf{K} = \sum_{e=1}^{n_e} \left(E_{min} + (E_0 - E_{min}) \left(\bar{\rho}_s^{(e)} \right)^p \right) \mathbf{k}_e \tag{1}$$

where $\mathbf{K}$ is the global stiffness matrix (for the in-plane or out-of-plane case), E_{min} is a very small stiffness used to avoid singularities in the global stiffness

matrix, E_0 is the stiffness of the solid material (silicon in our case), p is the penalization exponent that usually takes the value $p = 3$, and $\mathbf{k}_e$ is the elemental stiffness matrix (in-plane or out-of-plane) of an element. $\mathbf{K}$ is computed as the assembly of the n_e elements, so eq.(1) is not a summation in the classical sense, but in the assembling sense. The expression for the elemental stiffness matrix via FEM ([25]) would be:

$$\mathbf{k}_e = \int_{V_e} \mathbf{B}_e^T \mathbf{E} \mathbf{B}_e \, \mathrm{d}V$$

where $\mathbf{E}$ is the material property matrix, V_e is the finite element and $\mathbf{B}$ is the usual FE strain-displacement matrix that will adopt an expression or another depending on each case (in-plane or out-of-plane). In the in-plane case we have used bilinear elements with eight degrees of freedom per element ($\mathbf{B}$ is 3 by 8). In the out-of-plane one we have used Kirchhoff plate elements with 12 degrees of freedom per element ($\mathbf{B}$ is 3 by 12), see [25].

Special attention should be paid to the discrete expression for the global force vector:

$$\mathbf{F} = \sum_{e=1}^{n_e} \rho_p^{(e)} R(\bar{\rho}_s^{(e)}) \mathbf{f}_e$$

$R(\bar{\rho}_s^{(e)}) = \left(\bar{\rho}_s^{(e)}\right)^3$ is an interpolation scheme used to penalize the piezoelectric force in those elements where there is no piezoelectric layer. This scheme is needed to model the piezoelectric force in the void elements. Different schemes with the same purpose have been successfully used in [11] and [26].

At this point, remember that when working with a symmetric laminated structure (Fig.3 (a)) and assuming perfect bonding between layers, the distribution of the strain of the plate depends on the polarization of the piezoelectric layers. For an in-phase polarization (both piezo layers are polarized in the same direction), the strain across the thickness is constant:

$$\varepsilon(z) = \varepsilon_0$$

where ε_0 is the initial strain produced by the piezoelectric effect. For an out-of-phase polarization (piezo layers are polarized in opposite directions), the strain

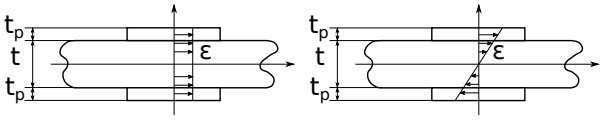

(a) In-phase (left) and out-of-phase (right) polarization

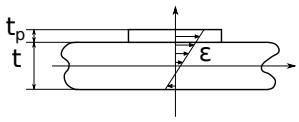

(b) One-phase polarization

Figure 3: Strain for a symmetric (top) and unsymmetric (bottom) laminate.

follows a linear distribution across the thickness:

$$\varepsilon(z) = \alpha z$$

where z is the height and α is a constant that represents the slope of the distribution. In such a case the piezoelectric effect produces a pure bending moment, whose expression is

$$M = E_0 I \alpha$$

where I is the moment of inertia.

By contrast, in the case of an unsymmetrical laminated plate (Fig.3 (b)) the expression of the strain is different:

$$\varepsilon(z) = \alpha z + \varepsilon_0$$

In such a case, the piezoelectric force generates a moment M_0, that makes the plate bend, and a initial strain ε_0 that extends or contracts the plate (see Fig. 4). All expressions as well as the computations of both the flexural and extensional components can be found in [27] and [28].

3. Robust formulation

As it was mentioned above, it is very common that the manufactured designs are subject to fabrication errors, specially at the micro-scale. It would

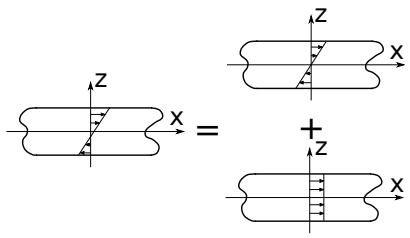

Figure 4: Decomposition of an unsymmetric strain distribution.

be desirable to minimize the sensitivity of the goal (the in-plane displacement in our case) to small changes in the volume fraction. A possible way to do that is by using the robust topology optimization approach ([14] and [29]). The method consists in a min max formulation where the worst performing design is minimized. Each one of those designs is regularized by using different projection schemes: dilated ($\tilde{\boldsymbol{\rho}}^d$), intermediate ($\tilde{\boldsymbol{\rho}}^i$) and eroded ($\tilde{\boldsymbol{\rho}}^e$), with thresholds η, 0.5 and $1-\eta$, respectively. From now on, the super index q indicates the type of projection, that is, e for the eroded, i for the intermediate and d for the dilated.

The design problem now formulated in terms of the robust approach may be expressed as:

$$\max_{\boldsymbol{\rho}_s,\boldsymbol{\rho}_p} \min\{u_1^e(\bar{\boldsymbol{\rho}}_s^e(\boldsymbol{\rho}_s),\boldsymbol{\rho}_p), u_1^i(\bar{\boldsymbol{\rho}}_s^i(\boldsymbol{\rho}_s),\boldsymbol{\rho}_p), u_1^d(\bar{\boldsymbol{\rho}}_s^d(\boldsymbol{\rho}_s),\boldsymbol{\rho}_p)\} \tag{2}$$

s.t.: *In-plane and out-of-plane equilibrium equations:*

$$\begin{cases} \left(\mathbf{K}_i^q(\bar{\boldsymbol{\rho}}_s^q) + \mathbf{1}_{out}k_{out}\right)\mathbf{U}_i^q = \mathbf{F}_i^q(\bar{\boldsymbol{\rho}}_s^q,\boldsymbol{\rho}_p),\ q \equiv e,i,d \\ \mathbf{K}_o^q(\bar{\boldsymbol{\rho}}_s^q)\mathbf{U}_o^q = \mathbf{F}_o^q(\bar{\boldsymbol{\rho}}_s^q,\boldsymbol{\rho}_p),\ q \equiv e,i,d \end{cases}$$

Displacements at the jaws:

$$\begin{cases} u_1^q = \mathbf{L}_1^T\mathbf{U}_i^q,\ q \equiv e,i,d \\ u_2^q = \mathbf{L}_2^T\mathbf{U}_o^q,\ q \equiv e,i,d \\ u_3^q = \mathbf{L}_3^T\mathbf{U}_o^q,\ q \equiv e,i,d \end{cases}$$

Constraints:

$$\begin{cases} (u_2^q)^2 \leq \varepsilon_d^2 (u_1^q)^2, \ q \equiv e, i, d \\ (u_3^q)^2 \leq \varepsilon_d^2 (u_1^q)^2, \ q \equiv e, i, d \\ \mathbf{1}^T \bar{\boldsymbol{\rho}}_s^d \leq V_d^* \\ \boldsymbol{\rho}_s \in [0, 1] \\ \boldsymbol{\rho}_p \in [-1, 1], \end{cases} \tag{3}$$

where V_d^* is the maximum volume constraint computed over the dilated design. The expression for this volume would be

$$V_d^* = \frac{V^*}{V_i} V_d$$

where V_i and V_d are the volume fractions for the intermediate and dilated designs, respectively, and V^* is the prescribed maximum volume fraction for the intermediate design. This value will be updated during the optimization process.

As max function is not differentiable, the optimization problem showed above is typically reformulated using the so-called bound formulation ([30]). The objective function (2) is replaced by

$$\max_{\boldsymbol{\rho}_s, \boldsymbol{\rho}_p} : \quad \lambda,$$

and a new constraint is added to (3)

$$u_1^q \geq \lambda, \ q \equiv e, i, d$$

where λ is an additional variable that does not depend on the other variables of the problem $\bar{\boldsymbol{\rho}}_s$ and $\boldsymbol{\rho}_p$, and helps us to circumvent the issue of the non-differentiability of the max-min problem.

4. Numerical implementation

In this section, the numerical algorithm used to solve this problem is presented. We can find in the literature two kinds of methods to solve an optimization problem: optimality criteria methods, that use optimality conditions, and descent methods, based on the gradient information. In this work the optimizer used is the MMA ("Method of Moving Asymptotes") [31], that belongs to

the second group. Descent methods require information about the sensitivities of the objective function and constraints, but these computations are straightforward for this particular problem and that is the reason why they are not included here.

The optimization algorithm in a pseudo code may look like:

1. Choose the dimensions of the plate and the properties of the materials that will be used. We need to fix the points where the displacement is maximized and the ones where it is suppressed. Also, the value of the parameter ε_d must be fixed as well as the output spring k_{out}.
2. Initialize both design variables $\boldsymbol{\rho}_s$ and $\boldsymbol{\rho}_p$.
3. Compute the physical density $\bar{\boldsymbol{\rho}}_s$ by filtering and projecting the initial structural density $\boldsymbol{\rho}_s$.
4. Solve the 6 finite element problems (3 in-plane and 3 out-of-plane for each one of the projections), and extract the displacements to be optimized and suppressed from the global vectors of displacements.
5. Compute the constraints.
6. Compute the sensitivities of the objective function and the constraints.
7. Update design variables by using the MMA.
8. Check the stop criteria, until convergence update the value of β and go back to step 3 .

Once the problem has been solved, we plot the design variables. It is important to remark that in order to save computation time and thanks to the symmetry of our problem, only the half of the domain is simulated.

5. Numerical examples

In this section, some optimal microgripper-type actuators are presented. The software used to solve this problem is programmed by Matlab and afterwards the physical behaviour is checked by CoventorWare. The domain where the problem is solved is a square in all the examples, with dimensions as shown in Fig.(2).

Fixed passive areas of void material are fixed at the jaws in order to have enough space to grab the objects. The domain is discretized with a different number of elements depending on the size of the plate. The material of the host layer is silicon, and the one of the piezoelectric layer is AlN. The Young's modulus of the silicon is 130GPa (the stiffness of the piezoelectric layer is neglected). The stiffness of the void area is set to 130Pa (negligible compared with the silicon Young's modulus) in order to avoid singularities in the stiffness matrix. The Poisson's ratio is 0.28 for both materials. The thickness of the layers are 10μm for the silicon and 1μm for the AlN, respectively. The piezoelectric constant of the AlN is $d_{31} = 2 \times 10^{-12}$pm/V. The input of the problem is a voltage of 10V and the relationship ε_d between the suppressed and the optimized displacements is fixed to 1%. At this point it is important to remind that only the half of the domain needs to be simulated thanks to the symmetry of the problem. Concerning geometrical constants, the length L of the domain will change in the different examples, the length and the height of the passive area are set to $L_p = 1000\mu$m and $h_p = 50\mu$m, respectively. Finally, the separation between the two points where the bending in cancelled is 25μm. The minimum length scale can be controlled by fixing the radius filter r and the value of the threshold η. This feature size is fixed to 250μm in all the examples except two where this value is changed in order to analyse the results.

In the first example the length of the square is set to 5000μm. The mesh used in this case is 200 by 200 elements, which means 40000 elements. The stiffness of the spring is set to $k_{out} = 20$N/m. The optimized design of the structure and the electrode profile for each projection is shown in Fig.(5). The structure layout is shown in Fig.(5)(left), where black and white means solid and void areas. At this point it is important to remark that there are no gray areas, which means that the robust topology optimization scheme is working correctly. The electrode profile is presented in Fig.(5)(right). Orange and blue colors represent parts of the structure with different polarity. It is noticed that the whole structure is being covered by electrode, otherwise it would not be electrically affected. In this example the three projections (erode, intermediate and dilate) are shown,

but from now on only the intermediate design will be shown. The measurement of the minimum length scale is done over the intermediate designs (the one that would be fabricated, also called blue print design) as commented in [14]. The displacement at the output port (in the intermediate design) is 2.46μm for this example. The suppressed bending at the interest points is smaller than the 1% of the maximized displacement.

Fig.(6) shows the result of such calculation for the device in Fig.(5)(b). As can be seen, the adapted design shows a non-zero out-of-plane displacement near the jaw, far from the anchors, where the effect of the bending is higher. This vertical displacement, although lower than the in-plane displacement (0.3 and 0.5 microns, respectively, for 10V), is not negligible as in the ideal design, but clearly demonstrates the potential of our model to limit the bending of actuators fabricated with one single piezoelectric film on top of the structure.

Fig.(7) shows optimized designs for a spring value of $k_{out} = 100$N/m (left) and $k_{out} = 200$N/m (right). The electrode profile contains all the information, then for the sake of simplicity the structure layout $\boldsymbol{\rho}_s$ does not need to be shown. It is easy to check that the minimum length scale imposed is ensured in the whole design. The displacements in these cases are 1.66μm and 1.34μm, respectively. The increasing of the value of k_{out} also implies an increase of the stiffness of the structure, which explains the optimized displacement reduction.

Squared domains of different sizes are presented in Fig.(8). The length is fixed to 3000μm in the left design, and 8000μm in the right one. In both cases the radius filter is fixed to 250μm. The mesh used for the size $L = 3000\mu$m is 240×240 elements and the one use for $L = 8000\mu$m is 320×320 elements. The output displacement is 1.24μm in the first case and 5.00μm in the second one. The deformation at the output port is bigger than in the second case because the size of the plate is bigger. A bigger size means a bigger surface covered by the electrode, then increasing the piezoelectric force generated. At first sight, the minimum length scale seems to be smaller in the second design, but the longer size of the plate must be taken into account.

To finish, the effect of varying the minimum length scale is shown in Fig.(9)

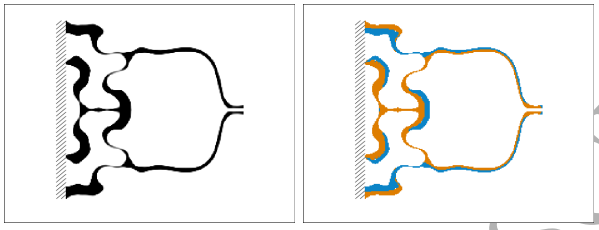

(a) Erode projection

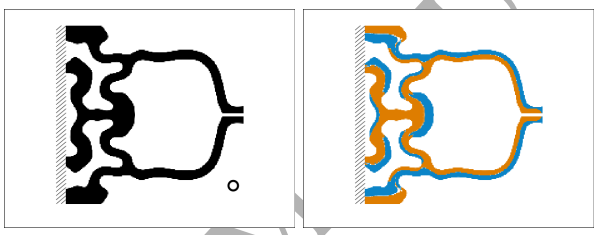

(b) Intermediate projection

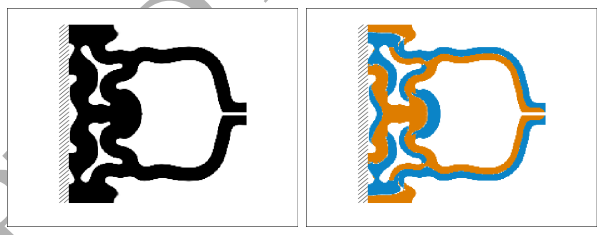

(c) Dilate projection

Figure 5: Structure variables $\boldsymbol{\rho}_s$ (left) and electrode profile $\boldsymbol{\rho}_p$ (right) for the three different projections. The circle in the intermediate design indicates the minimum length scale that is set to 250μm for this example.

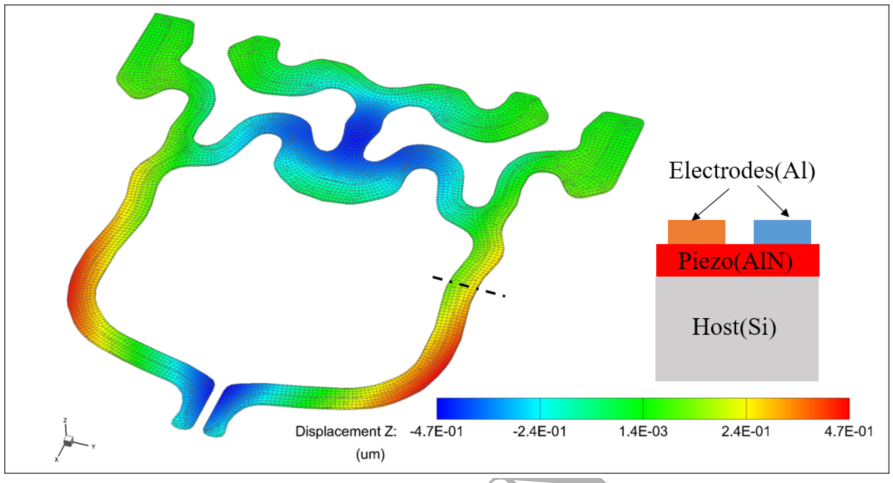

(a) Undeformed gripper.

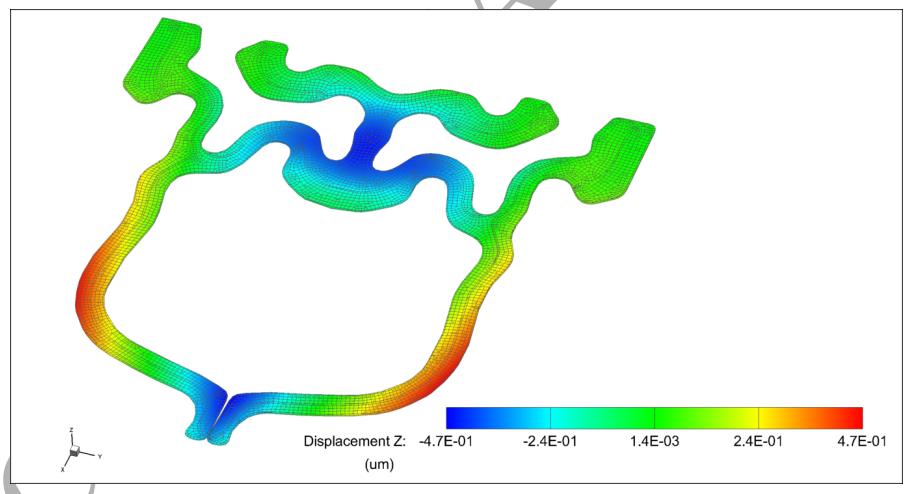

(b) Deformed gripper.

Figure 6: Result of the 3D modelling with the FEM software, with colors showing the out-of-plane displacement. The inset corresponds to a cross section along the dotted line, remarking the spacing between electrodes.

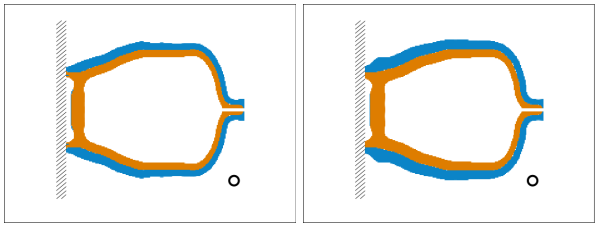

Figure 7: Electrode profile for $L = 5000\mu$m and $k_{out} = 100$N/m (left) and $k_{out} = 200$N/m (right).

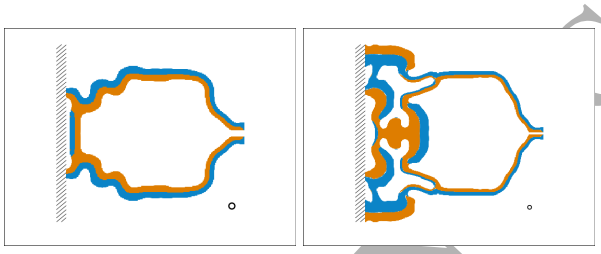

Figure 8: Electrode profile for $L = 3000\mu$m (left) and $L = 8000\mu$m (right) and $k_{out} = 20$N/m.

with $L = 8000\mu$m. The radius filter is changed to 160μm (left) and 340μm (right) and the displacement at the output port is 6.09μm and 4.46μm, respectively. When the radius decreases, smaller parts of the structure appear and the displacement at the output port tends to increase. Somehow the minimum length scale can be understood as a constraint. When a bigger length scale is imposed, the constraint is more restrictive and then the value of the objective function in the optimal design is smaller.

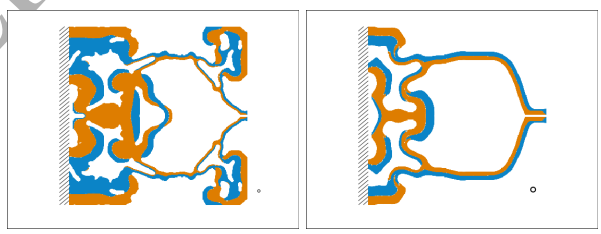

Figure 9: Electrode profile for $L = 8000\mu$m and $r_{min} = 70\mu$m (left) and $r_{min} = 154\mu$m (right).

6. Conclusions

A microgripper-type actuator has been designed by using the topology optimization method. The main novelty of this work is the suppression of the bending of the microactuator at some points of interest while the in-plane displacement is maximized through the gripping effect. This goal has been achieved adding some constraints over the out-of-plane displacement at these points. The suppression of this bending is important in this kind of actuators, otherwise the transducer could not grab the object. In this work some design parameters (size of the squared domain, output stiffness, etc.) have taken different values in order to compare different designs. The deformation of the whole structure has been checked with a simulation software, CoventorWare, ensuring that the model used is working as expected. The optimal design with the best behaviour will be fabricated and tested.

Other issue is the appearance of large gray areas (somehow related to the physics of the problem), which have been successfully overcome by using robust topology optimization and a proposed interpolation scheme altogether.

In addition, a robust formulation has been used with two objectives. The first goal is to control the minimum length scale that appears in the optimal designs. The second one is to minimize the effect of fabrication errors. It is worthwhile emphasizing that this approach is valid as long as the deformation of the structure is small compared with the length of the plate. In case of using other kind of materials, e.g. polymers, a non-linear model must be used in order to model correctly large deformations. The results of this investigation will be published in [15].

Acknowledgements

The work of J.C. Bellido and A. Donoso has been funded by MINECO (Spain) through grant MTM2013-47053-P and Junta de Comunidades de Castilla-La Mancha (Spain) through grant PEII-2014-010-P. The work of O. Sigmund has been supported by the research project 'Sapere Aude TOpTEn' (Topology

Optimization of Thermal ENergy systems) from the Danish Council for Independent Research, grant: DFF-4005-00320. The work of J.L. Sánchez-Rojas was supported by Spanish MINECO project TEC2015-67470-P and regional JCCM project PEIC-2014-001-P.

References

[1] O. Sigmund, S. Torquato, I. A. Aksay, On the design of 1-3 piezo-composites using topology optimization, J Mater Res 13 (4) (1998) 1038–1048.

[2] E. C. N. Silva, N. Kikuchi, Design of piezoelectric transducers using topology optimization, Smart Mater Struct 8 (3) (1999) 350–364.

[3] M. Kögl, E. C. N. Silva, Topology optimization of smart structures: design of piezoelectric plate and shell actuators, Smart Mater Struct 14 (2) (2005) 387–399.

[4] R. C. Carbonari, E. C. N. Silva, S. Nishiwaki, Optimum placement of piezoelectric material in piezoactuator design, Smart Mater Struct 16 (1) (2007) 207–220.

[5] Z. Luo, W. Gao, C. Song, Design of multi-phase piezoelectric actuators, J Intell Mater Syst Struct 21 (18) (2010) 1851–1865.

[6] Z. Kang, L. Tong, Integrated optimization of material layout and control voltage for piezoelectric laminated plates, J Intell Mater Syst Struct 19 (2008) 889–904.

[7] Z. Kang, L. Tong, Topology optimization-based distribution design of actuation voltage in static shape control of plates, Comput Struct 86 (19-20) (2008) 1885–1893.

[8] Z. Kang, R. Wang, L. Tong, Combined optimization of bi-material structural layout and voltage distribution for in-plane piezoelectric actuation, Comput Methods Appl Mech Engrg 200 (13-16) (2011) 1467–1478.

[9] Z. Kang, X. Wang, Z. Luo, Topology optimization for static shape control of piezoelectric plates with penalization on intermediate actuation voltage, J Mech Des 134 (5) (2012) 051006.

[10] A. Molter, J. S. O. Fonseca, L. dos Santos Fernandez, Simultaneous topology optimization of structure and piezoelectric actuators distribution, Applied Mathematical Modelling 40 (9-10) (2016) 5576 – 5588.

[11] D. Ruiz, J. C. Bellido, A. Donoso, J. L. Sánchez-Rojas, Design of in-plane piezoelectric sensors for static response by simultaneously optimizing the host structure and the electrode profile, Struct Multidisc Optim 48 (5) (2013) 1023–1026.

[12] D. Ruiz, J. C. Bellido, A. Donoso, Design of piezoelectric modal filters by simultaneously optimizing the structure layout and the electrode profile, Struct Multidisc Optim 53 (2016) 715 – 730.

[13] M. Kucera, E. Wistrela, G. Pfusterschmied, V. Ruiz-Díez, T. Manzaneque, J. Hernando-García, J. L. Sánchez-Rojas, A. Jachimowicz, J. Schalko, A. Bittner, U. Schmid, Design-dependent performance of self-actuated and self-sensing piezoelectric-aln cantilevers in liquid media oscillating in the fundamental in-plane bending mode, Sens Act B Chem 200 (2014) 235 – 244.

[14] F. Wang, B. S. Lazarov, O. Sigmund, On projection methods, convergence and robust formulations in topology optimization, Struct Multidisc Optim 43 (6) (2011) 767–784.

[15] D. Ruiz, O. Sigmund, Optimal design of robust piezoelectric microgrippers under large displacements, Work in progress.

[16] A. Donoso, J. C. Bellido, Systematic design of distributed piezoelectric modal sensors/actuators for rectangular plates by optimizing the polarization profile, Struct Multidisc Optim 38 (4) (2009) 347–356.

[17] P. H. Destuynder, I. Legrain, L. Castel, N. Richard, Theoretical, numerical and experimental discussion of the use of piezoelectric devices for control-structures interaction, Euro J Mech 11 (2) (1992) 181–213.

[18] H. T. Banks, R. Smith, Y. Wang, Modeling of piezoceramic patch interactions with shells, plates and beams, Appl Math 53 (1995) 353–381.

[19] T. E. Bruns, D. A. Tortorelli, Topology optimization of non-linear elastic structures and compliant mechanisms, Comput Methods Appl Mech Engrg 190 (26-27) (2001) 3443–3459.

[20] B. Bourdin, Filters in topology optimization, Int J Numer Meth Engng 50 (9) (2001) 2143–2158.

[21] J. K. Guest, J. H. Prvost, T. Belytschko, Achieving minimum length scale in topology optimization using nodal design variables and projection functions, Int J Numer Meth Engng 61 (2) (2004) 238–254.

[22] O. Sigmund, Morphology-based black and white filters for topology optimization, Struct Multidisc Optim 33 (4-5) (2007) 401–424.

[23] O. Sigmund, Manufacturing tolerant topology optimization, Acta Mech Sin 25 (2) (2009) 227–239.

[24] M. P. Bendsøe, O. Sigmund, Material interpolation schemes in topology optimization, Arch Appl Mech 69 (9-10) (1999) 635–654.

[25] E. Oñate, Cálculo de Estructuras por el Método de Elementos Finitos, Análisis estático lineal, 2nd Edition, CIMNE, 1995.

[26] D. Ruiz, A. Donoso, J. C. Bellido, M. Kucera, U. Schmid, J. L. Sánchez-Rojas, Design of piezoelectric microtransducers based on the topology optimization method, Microsyst Technol 22 (7) (2016) 1733–1740.

[27] S. O. Moheimani, A. J. Fleming, Piezoelectric Transducers for Vibration Control and Damping, 2st Edition, Springer, 2006.

[28] G. P. Gibbs, C. R. Fuller, Excitation of thin beams using asymmetric piezoelectric actuators, J Acoust Soc Am 92 (6) (1992) 3221–3227.

[29] F. Wang, J. S. Jensen, O. Sigmund, Robust topology optimization of photonic crystal waveguides with tailored dispersion properties, J Opt Soc Am B 28 (3) (2011) 387–397.

[30] N. L. Pedersen, Maximization of eigenvalues using topology optimization, Struct Multidisc Optim 20 (2000) 2–11.

[31] K. Svanberg, The method of moving asymptotes-a new method for structural optimization, Int J Numer Meth Engng 24 (2) (1987) 359–373.